JGR Biogeosciences

RESEARCH ARTICLE
10.1029/2020JG006054

Influence of Hydraulic Connectivity on Carbon Burial Efficiency in Mackenzie Delta Lake Sediments

J. Lattaud[1], L. Bröder[1], N. Haghipour[1,2], J. Rickli[3], L. Giosan[4], and T. I. Eglinton[1]

[1]Department of Earth Sciences, Biogeoscience Group, ETH Zurich, Zurich, Switzerland, [2]Laboratory of Ion Beam Physics, ETH Zurich, Zurich, Switzerland, [3]Department of Earth Sciences, Institute of Geochemistry and Petrology, ETH Zurich, Zurich, Switzerland, [4]Geology and Geophysics, Woods Hole Oceanographic Institution (WHOI), Woods Hole, MA, USA

Key Points:

- High-closure lake bury very little petrogenic hydrocarbons in contrast to no- and low-closure lakes
- High closure lakes have higher organic carbon loadings than usually found in freshwater systems
- We found no evidence for a significant change in carbon burial in the lakes over the last 200 years

Supporting Information:

- Supporting Information S1
- Data Set S1
- Data Set S2
- Data Set S3

Correspondence to:
J. Lattaud,
Jlattaud@ethz.ch

Citation:
Lattaud, J., Bröder, L., Haghipour, N., Rickli, J., Giosan, L., & Eglinton, T. I. (2021). Influence of hydraulic connectivity on carbon burial efficiency in Mackenzie Delta lake sediments. *Journal of Geophysical Research: Biogeosciences*, *126*, e2020JG006054. https://doi.org/10.1029/2020JG006054

Received 3 SEP 2020
Accepted 24 JAN 2021

Abstract The Arctic is undergoing accelerated changes in response to ongoing modifications to the climate system, and there is a need for local to regional scale records of past climate variability in order to put these changes into context. The Mackenzie Delta region in northern Canada is populated by numerous small shallow lakes. They are classified as no-, low-, and high-closure (NC, LC, and HC, respectively) lakes, reflecting varying degrees of connection to the river main stem, and have different sedimentation characteristics. This study examines sedimentological (mineral surface area, grain size), carbon isotopic (bulk and molecular-level) and inorganic isotopic (neodymium) characteristics of sediment cores from three lakes representing each class. We find that HC lake sediments exhibit strikingly different properties from the other lake sediments. Specifically, they are characterized by higher organic carbon loadings per unit mineral surface area and with relatively minor influence from allochthonous, petrogenic (rock-derived) organic carbon. In contrast, LC and NC lakes have the potential to record basin-scale climatic changes at a high resolution by virtue of enhanced detrital sedimentation. Overall the delta lakes have the capacity to bury about 2 MtC year^{-1}, with little changes in the last 200 years. However, in the (near) future, an increased number of high closure lakes might change the carbon burial efficiency of the Mackenzie Delta as they seem to retain less carbon than NC and LC lakes.

Plain language summary The Arctic is rapidly warming compared to other parts of the world, yet the consequences on regional aquatic carbon cycling are unknown. We studied the properties of sediment cores from three different types of lakes within the Mackenzie River Delta to examine relationships between the degree of lake connectivity with the main river channel network and carbon inputs and burial. "High-closure" lakes that are rarely connected to the river mainstem are markedly different from those that are frequently inundated by the river. Their organic carbon is of local origin, in contrast to the carbon in more connected lakes. Moreover, despite higher carbon contents, high closure lakes bury carbon less efficiently, suggesting that an increase in the abundance of these lakes would lead to a reduction in carbon burial in the delta. No significant changes in carbon burial are, however, apparent in lake sediment records spanning the last ~200 years.

1. Introduction

Inland water bodies, such as lakes, ponds, wetlands, and rivers link the terrestrial realm to the ocean and, although covering a small portion of Earth's surface, play an integral role in modulating Earth's carbon fluxes (e.g., Aufdenkampe et al., 2011; Battin et al., 2009; Raymond et al., 2013; Tranvik et al., 2009, 2018). Furthermore, the water cycle is highly sensitive to climate change, impacting the fluxes through dynamics of hydrological networks throughout the land-ocean aquatic continuum. As the carbon cycle is intertwined with the water cycle, both are expected to be significantly altered by—and contribute to—climate change (Battin et al., 2009; Ward et al., 2017). Lakes are dynamic environments where carbon is transported, deposited, buried and/or oxidized, and where changes are amplified on short timescales (Tranvik et al., 2009). Organic carbon burial in lake sediments comprises an important long-term carbon sink, with rapid removal of carbon from surface reservoirs and efficient sequestration in underlying sediments (Sobek et al., 2009; Tranvik et al., 2009).

Although lakes occupy only 2% of the Earth's surface, carbon burial in lake sediments corresponds to ~50% of the burial in ocean sediments that cover 71% of the Earth's surface (Cole et al., 2007; Dean &

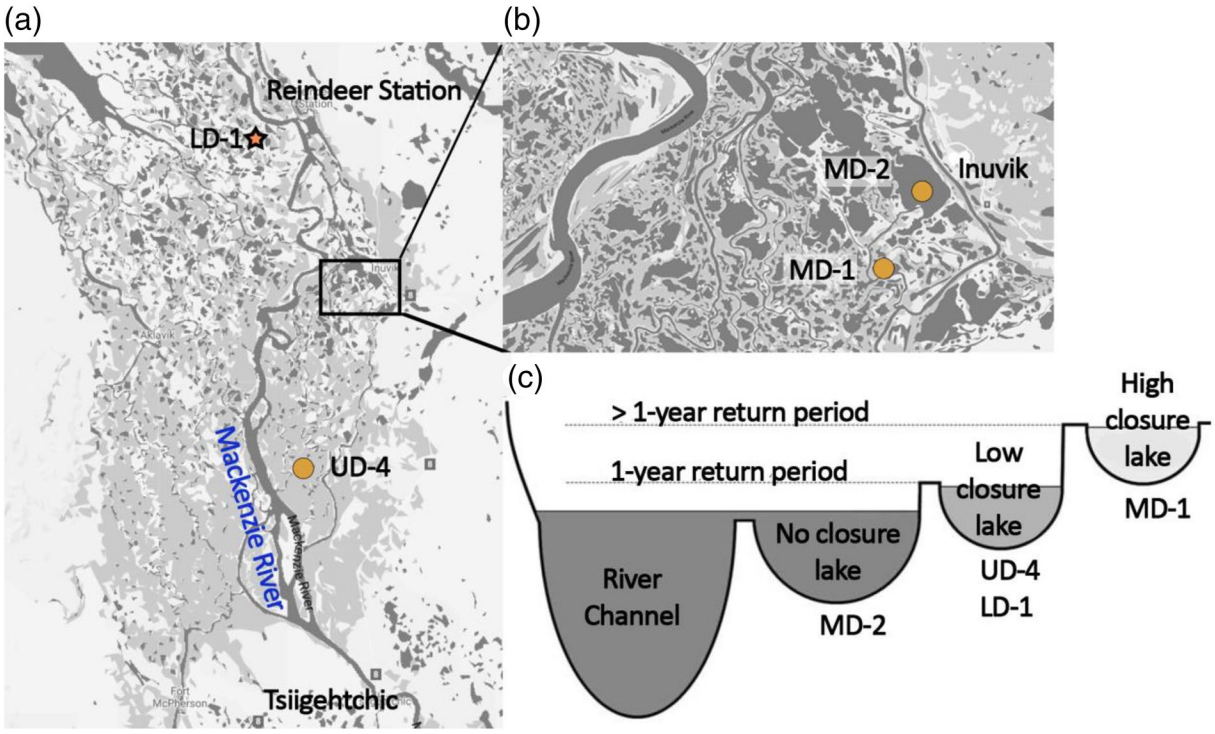

Figure 1. Localization of the Mackenzie Delta lakes (a) global view of the Mackenzie River Delta, (b) zoom into the Inuvik area and (c) lake classification (adapted from Tank et al., 2009). Lakes UD-4, MD-1 and MD-2 were studied in this work. Vonk et al. (2015b) reported on lake LD-1, a low closure lake similar to UD-4.

Gorham, 1998). However, lake ecosystems are fueled by terrestrial carbon which fosters heterotrophic organisms and thus the outgassing of methane (CH_4) and carbon dioxide (CO_2). Most lakes globally are supersaturated in CO_2 compared to the atmosphere (Sobek et al., 2005) and lakes containing anoxic waters and those that are largely vegetated are significant CH_4 emitters (Bastviken et al., 2011). As such, lakes are usually considered as net sources of carbon to the atmosphere, while also serving as loci of enhanced carbon burial (Cole et al., 2007).

Due to thaw and subsidence of previously frozen ground (permafrost), which creates shallow depressions, Arctic deltas are characterized by a high number of lakes and ponds (Raymond et al., 2013; Sobek et al., 2005). The permafrost related generation of shallow depressions is known as thermokarst (e.g., Vonk, Tank et al., 2015). Arctic inland waters can represent both a source and sink of CO_2 and CH_4, depending on the balance between emission of preaged carbon (released by permafrost thaw and microbially remineralized) and carbon fixation (both autotrophic and heterotrophic) by aquatic ecosystems. The Mackenzie River Delta is the most extensive in North America covering 12,170 km^2 (Droppo et al., 1998), and is host to many thousands of small, shallow lakes (<10 ha in area and <4 m deep, Emmerton et al., 2007). These deltaic lakes can be broadly classified into three categories: no closure (NC, continuously connected to the river), low closure (LC, connected during the annual spring flood), and high closure (HC, connected less than annually, during strong spring flood events) (Figure 1, Lesack & Marsh, 2007). Small shallow lakes are thought to be zones of important primary production when light availability is high, that is, turbidity is low, and nutrient availability is not limiting (Tranvik et al., 2009), leading to high annual carbon burial rates (up to 17,000 gCm^{-2} $year^{-1}$, Downing et al., 2008). The different types of lakes within the Mackenzie River Delta, reflecting variations in hydraulic connectivity and thus nutrient and sediment supply, may capture different facets of local and regional-scale carbon and hydrological cycling. Moreover, as some HC lakes are thermokarst-influenced, on-going thawing of underlying permafrost releases preaged carbon, CO_2 and CH_4, to the water column, influencing the carbon balance. Tank et al. (2008) found that HC and LC lakes are a net sink of CO_2, especially in summer, primarily due to their extensive macrophyte cover. However, they are strong CH_4 emitters due to methanogenetic ebullitive transport during winter with the development of

water column anoxia. As for much of the Arctic region, the Mackenzie River region is expected to undergo marked environmental modifications as a result of on-going climate change (Richter-Menge et al., 2019). With earlier melting of river ice, the annual flood pulse (freshet) may decline or become damped, potentially resulting in disconnection of some lakes from the river, and leading to their subsequent desiccation (Lesack & Marsh, 2010; Lesack et al., 2014). In contrast, overall riverine discharge is projected to increase as a consequence of increased precipitation in the Mackenzie River catchment (Peterson et al., 2002, 2006) which may enhance lower-altitude lake connectivity. Stronger or prolonged connection to the river and associated permafrost thaw, may amplify thermokarst processes which in turn may reduce the lakes' effectiveness as CO_2 sink, potentially altering greenhouse gas emissions to the atmosphere.

Previous studies on Mackenzie Delta lakes have examined inorganic and organic properties of surface sediments from a subset of lakes, spatially distributed across the delta (Peterse et al., 2014; Vonk, Giosan et al., 2015). Furthermore, a sediment core from one LC lake (LD-1) was studied in detail from the perspective of its value as an archive of past river flooding and climatic change, and in terms of vascular plant carbon input (Vonk et al., 2016, 2019). Here, we seek to establish links between the biogeochemical characteristics and the hydraulic connectivity of arctic deltaic lakes. We examine geochemical and sedimentological properties of three sediment cores collected from a NC, LC, and HC lake from the middle and upper Mackenzie Delta. In order to assess past changes in carbon and nutrient supply to these lakes, and their impact on lacustrine carbon cycles (Tranvik et al., 2009), we compare and contrast organic and inorganic isotopic characteristics to elucidate carbon and sediment sources to the lakes. Biogeochemical and sedimentological characteristics are interpreted in the context of differences in lake connectivity, and their potential to record both distal (NC, river-derived) and local (HC, lake catchment-derived) variability. The chosen lakes are meant to highlight differences and similarities between the three types of connectivity.

2. Material and Methods

2.1. Setting and Sampling of Lakes

The Mackenzie River is the largest Arctic river of North America and the largest single source of sediment and carbon to the Arctic Ocean, with an mean water discharge of about 320 km^3 $year^{-1}$ carrying about 1 MtC $year^{-1}$ (Droppo et al., 1998). As for other Arctic rivers, the hydrological cycle of the Mackenzie is dominated by the freshet, that is, melting of snow and ice, which occurs in early June and accounts for more than 60% of the annual water and about 90% of the sediment discharge (Drenzek et al., 2007). A large fraction of the catchment of the Mackenzie and its tributaries is underlain by continuous (13%) or discontinuous permafrost (69%; Amon et al., 2012; Droppo et al., 1998; Holmes et al., 2012). The river remains under ice cover from late September until early June. The freshet brings nutrients to the delta lakes and, in combination with initially shallow water levels, initiates a massive bloom of submerged macrophytes (mainly *Potamogeton* spp., Squires & Lesack, 2002), resulting in CO_2 depletion and elevated pH in HC, and some LC lakes during summer (Tank et al., 2008, 2009). In most of the deltaic lakes, phytoplankton production is negligible (Squires & Lesack, 2002). During winter, under the ice cover, anoxia develops in HC and LC lakes following the decay of macrophytes, resulting in sulfate reduction and CH_4 release, as well as an increase in pCO_2 (Squires et al., 2009). In addition, the Mackenzie Delta area is known to receive large amounts of "old" petrogenic (originating from the Canol Formation) and preaged permafrost hydrocarbons, which is more or less efficiently buried in lake sediments depending on the lake connection to the river (Goñi et al., 2005; Hilton et al., 2015; Vonk et al., 2019; Yunker et al., 1993). Sedimentation rates are typically lower for HC lakes than for NC and LC lakes (Marsh et al., 1999), with some lakes presenting characteristic lamination with a darker thick layer from the spring freshet and a finer lighter layer deposited during the summer months (Vonk et al, 2015, 2016). Radiogenic neodymium isotope ratios ($^{143}Nd/^{144}Nd$ expressed as εNd) in lake sediments of the Mackenzie Delta region are a good tracer of source rocks, with the western part of the delta exhibiting more radiogenic values, typical of the Peel Plateau, than the eastern part being sourced predominately from the older Devonian Canol Formation (Vonk, Giosan et al., 2015). Specifically, lake sediments in the western delta yield values of -12.15 ± 0.81 compared to values of -13.22 ± 0.45 in the east (Vonk, Giosan et al., 2015). There is also a South to North gradient, with more radiogenic values in the South likely due to the presence of coarser, more radiogenic grains (-12.80 ± 0.70 for lake sediments

of the upper delta) originating from the Peel and Arctic Red rivers, while in the northern part of the delta, only finer, less radiogenic grains remain (−13.85 ± 0.47 for lake sediments of the outer delta; Vonk, Giosan et al., 2015). Since the Great Slave Lake serves as a very efficient sediment trap, most of the sediments delivered to the Mackenzie Delta originate from the area north, that is, downstream, of this lake (Carson et al., 1998). The vegetation in the catchment of the Mackenzie River varies greatly: tundra, boreal forest, peatland and mountains (Dyke & Brooks, 2000), and the watershed is covered by lakes (10%), forest (35%), grassland (30%), and shrubland (10%) as well as minor cropland and wetland (Amon et al., 2012).

Twenty-six lake sediment cores were recovered from the Mackenzie Delta in March 2009 with a customized push-corer (built in-house at Woods Hole Oceanographic Institution, WHOI) as described by Vonk et al. (2015b). Cores were shipped and archived under refrigerated conditions, split lengthwise, with the working half of each core sliced into ∼1 cm sections. The three lake cores selected for this study (Figure 1) were described by Vonk et al. (2015b): MD-2 (NC, 68.358°N, 133.767°W), UD-4 (LC, 67.875°N, 134.175°W), and MD-1 (HC, 68.312°N, 133.835°W, previously named "NRC Lake," Squires et al., 2009). One core per lake was studied and the recovered core length was 1.47 m for MD-1 (HC), 1.88 m for MD-2 (NC) and 1.2 m for UD-4 (LC).

2.2. Bulk and Sedimentological Measurements

For the determination of bulk organic carbon (OC) properties, 10–15 mg of freeze-dried and homogenized sediment was fumigated with concentrated hydrochloric acid (HCl 37%) for 72 h at 60°C to remove inorganic carbon and subsequently neutralized and dried under a basic atmosphere (pH > 7, NaOH) at 60°C for another 72 h. Carbon isotopic compositions ($\delta^{13}C_{bulk}$, the ratio of $^{13}C/^{12}C$ in a sample relative to the standard Vienna PeeDee Belemnite, VPDB and $\Delta^{14}C_{bulk,}$ the ^{14}C isotopic ratio of a material relative to the modern standard after correction for fractionation to $\delta^{13}C_{bulk}$), total sediment OC (TOC) content and C/N ratios of bulk organic matter were measured with an Elemental Analyzer (EA) interface coupled to both a stable isotope analyzer (EA-IRMS, Elementar vario MICRO cube—Isoprime Precision) and Mini Carbon Dating System (MICADAS) accelerator mass spectrometer (AMS; McIntyre et al., 2016). $\Delta^{14}C$ values are corrected for blank, $\delta^{13}C$, year of coring (2009) and year of deposition. Date C.E. obtained from ^{14}C dating of wood are calibrated with the OxCal software using the IntCal13 (Reimer et al., 2013) calibration curve.

For mineral surface area (MSA) and grain size (GS) measurements, organic matter (OM) was removed from a freeze-dried sample aliquot (ca. 1 g) by combustion (12 h, 450°C, cool-down ramp −40°C h^{-1}) (Freymond et al., 2018). Before MSA measurement, samples were degassed under vacuum (>2 h, 350°C) to remove any remaining water and adsorbed gases. MSA was measured with N_2 using the BET method (Brunauer et al., 1938) with a 5-point adsorption isotherm (p/p_0 = 0.05–0.3) on a NOVA 4000 surface area analyzer (Keil et al., 1997). GS distributions were analyzed by laser diffraction on a Malvern Mastersizer 2000, where a sediment subsample was dispersed in sodium polyphosphate (1 gL^{-1}) and subsequently measured under ultrasonication (Freymond et al., 2018).

For Nd isotope analysis, sediment aliquots of 30–50 mg were weighed into 7 mL Teflon vials and treated repeatedly with aqua regia and nitric acid/hydrogen peroxide mixtures to oxidize organic compounds. These oxidation steps were performed before and after the digestion of the silicate fraction in a mixture of concentrated hydrofluoric and nitric acid (4 mL of 28.5 M HF, 1 mL of 14.5 M HNO_3) at 120°C for 3 days. Eventually the samples were brought up in 1 mL of 1 M HCl in preparation for ion chromatography. Pure Nd fractions were obtained combining a cation column to separate rare earth elements from the bulk sample matrix, followed by the isolation of Nd from other rare earth elements on LN spec (Pin & Zaldguegui, 1997). Total chemical blanks of ∼30 pg were negligible compared to sample Nd > 300 ng. Nd isotope compositions were measured on a Neptune Plus MC-ICP-MS at ETH Zurich in 2% HNO_3 at sample concentrations of 40–100 ppb. Instrumental mass bias correction followed Vance and Thirwall (2002). External reproducibility of the mass spectrometric analysis was monitored by repeated measurements of La Jolla (standard reference material) during the session and corresponded to < 10 ppm (2 SD, n = 15, run at 50 ppb). A more realistic error estimate from other sessions is somewhat larger at about 15 ppm. Sample isotope ratios were renormalized to the literature value for La Jolla ($^{143}Nd/^{144}Nd$ = 0.511856; Thirwall, 1991). The $^{143}Nd/^{144}Nd$

isotope ratios are expressed in epsilon-notation as relative deviations from the bulk silicate earth times 10'000 ($^{143}Nd/^{144}Nd = 0.512638$; Jacobsen & Wasserburg, 1980).

2.3. Lipid Extraction

Freeze-dried sediments (5–8 g) were treated three times with dichloromethane (DCM):Methanol (MeOH) (9:1, *v/v*) using an EDGE system (CEM). The total lipid extract was dried under a gentle stream of nitrogen (N_2) and then saponified with 0.5 M potassium hydroxide (KOH) in MeOH (2 h reflux at 70ºC). The neutral fraction was liquid-liquid extracted with hexane (four times) and then dried under N_2. This fraction was separated on a deactivated (1%) silica gel column into an apolar (containing *n*-alkanes), ketone and polar fraction, using hexane, hexane:DCM (9:1, *v/v*), and DCM:MeOH (1:1, *v/v*) as eluents, respectively. The remaining saponified products were acidified (pH ~ 1) prior to liquid-liquid extraction of long-chain fatty acids (with hexane:DCM, 4:1, *v/v*). The extract was then methylated overnight (12 h, 70°C) with MeOH:HCl (95:5, *v/v*), and the resulting fatty acid methyl esters (FAMEs) were liquid-liquid extracted four times with hexane. The FAME fraction was transferred into precombusted gas chromatography (GC) vials and dried under a stream of N_2. To quantify the compounds, a known amount of C_{36} *n*-alkane was added to the fractions.

2.4. Lipid Concentrations and Compound-specific $\delta^{13}C$ Analysis

FAMEs and *n*-alkanes were quantified on a HP 7890A gas chromatograph (GC) equipped with a flame ionization detector (FID), and a VF-1 MS capillary column (30 m × 0.25 mm, 0.25 μm film thickness). The temperature program started with a 1 min hold time at 50°C, followed by a 10°C min^{-1} ramp to 320°C and a 5 min hold time at 320°C. Peaks were identified against a mix of pure standard compounds based on retention time.

Before stable carbon isotope ($\delta^{13}C$, the ratio of $^{13}C/^{12}C$ in a sample relative to the standard Vienna PeeDee Belemnite, VPDB) analysis, the FAME fraction was further purified over a SiO_2 column with hexane:DCM (2:1, *v/v*) and DCM:MeOH (1:1, *v/v*). Compound-specific $\delta^{13}C$ analysis of FAMEs and *n*-alkanes was performed in duplicate by GC-isotope ratio mass spectrometry (GC–IRMS) on a Thermo Trace GC (1310) coupled with a Thermo Delta-V plus system. The GC was equipped with a RTX-200 MS capillary column (60 m × 0.25 mm i.d., 0.25 μm film thickness) and the temperature program was as follows: ramp from 40°C to 120°C at 40°C min^{-1}, followed by a 6°C min^{-1} ramp to 320°C and a 12 min hold time at 320°C.

The $\delta^{13}C$ value of the FAMEs have been corrected for carbon addition from methylation as follows (Equation 1):

$$\delta^{13}C_{\mathrm{FAME}} = \frac{\left(nC_{\mathrm{FAME}} + nC_{\mathrm{CH3}}\right) \times \delta^{13}C_{\mathrm{FAME}}\mathrm{measured} - nC_{\mathrm{CH3}} \times \delta^{13}C_{\mathrm{CH3}}}{nC_{\mathrm{FAME}}} \quad (1)$$

With nC_{FAME} = number of carbon atoms of FAME, $nC_{CH3} = 1$ and $\delta^{13}C_{\mathrm{CH3}} = -41.08 \pm 0.14$ ‰.

2.5. Lipid Ratios

Several ratios have been calculated to constrain *n*-alkane signatures. These include (Equation 2) the carbon preference index (CPI, Bray & Evans, 1961; Kvenvolden, 1966), which serves as an estimation of the proportion of sedimentary rock (petrogenic) or thermogenic hydrocarbons (~1 is indicative of ancient, thermally mature hydrocarbon inputs, and >5 for higher plant inputs; Collister et al., 1994; Equation 3) the average chain length of the *n*-alkanes and fatty acids (FA; average chain length (ACL), based on > C_{27} *n*-alkanes or > C_{24} FA; adapted from Eglinton & Hamilton, 1967), which can reflect the plant source, and (Equation 4) long-chain FA over long-chain *n*-alkane concentrations, indicative of preservation. Corresponding ratios are calculated according to:

$$\mathrm{CPI} = \frac{1}{2} \times \left(\frac{\sum_{i=12}^{16} C_{2i+1}}{\sum_{i=12}^{16} C_{2i}} + \frac{\sum_{i=12}^{16} C_{2i+1}}{\sum_{i=13}^{17} C_{2i}} \right) \quad (2)$$

$$\mathrm{ACL} = \frac{\sum_{i=27}^{33} i \times C_i}{\sum_{i=27}^{33} C_i} \quad (3)$$

$$\frac{\mathrm{LC}}{\mathrm{LC\ alkane}} = \frac{\sum_{i=26}^{30} \mathrm{FA}i}{\sum_{i=27}^{35} Ci} \quad (4)$$

where C*i* indicates the concentration of the compound *i*.

3. Results

3.1. Age-Depth Model

No closure (MD-2) and Low closure (UD-4): Horizons from Mackenzie River Delta sediment core were analyzed for ^{137}Cs activity as well as ^{210}Pb decay, as described in Graf Pannatier (1997) and Vonk et al. (2015b, 2016). Briefly, the onset of ^{137}Cs activity (corresponding to 1951 C.E.) was observed at different depths for each core, with the ^{137}Cs activity peak (corresponding to 1963 or 1964 C.E.; Rember et al., 1993) observed at 32.5 cm and 50 cm for UD-4 and MD-2, respectively (Figure S1). Resulting estimates for average sedimentation rates for UD-4 were 0.77 cm year^{-1} and 0.72 cm year^{-1} (1951–1964 C.E. and 1964–2009 C.E., respectively). For MD-2, sedimentation rates correspond to 0.62 cm year^{-1} (1951–1964 C.E.) and 1.1 cm year^{-1} (1964–2009 C.E.). Independent lamina counting agrees well with the number of annual laminations deducted from sedimentation rates. As such, the part of the core above the ^{137}Cs peak is dated based on lamina counting as well as sedimentation rate calculations. No apparent decay of ^{210}Pb is observed in the Mackenzie River Delta lake cores (Graf Pannatier, 1997), likely as a result of dilution due to high sedimentation rates. Significant vertical sediment reworking (e.g., due to bioturbation) is unlikely given the clear ^{137}Cs peaks (Figure S1). Sedimentation rates (pre or post^{137}Cs peak) are similar to those reported by Ferguson (1990) and Marsh and Hay (1999) for other LC and NC lakes in the region. ^{14}C measurements of plant fragments yielded ^{14}C-ages of 1742 ± 51 C.E. at 109 cm in UD-4 and 1825 ± 57 C.E. at 157 cm in MD-2. The ages of these wood fragments are ~100 years older than the calculated age based on sedimentation rates (1864 C.E. for UD-4 at 109 cm and 1904 C.E. for MD-2 at 157 cm), likely indicating preaging of the wood in soil/permafrost prior to deposition in the lake.

High closure (MD-1): Lake MD-1 was not measured for ^{137}Cs during this study, however previous studies (Ferguson, 1990; Marsh et al., 1999) reported a relatively smeared ^{137}Cs peak (at 4 cm in 1987 C.E., Figure S1). However, Ferguson (1990) and Mash and Hay (1999) suggested that the peak should still represent 1963–1964 C.E. The $\Delta^{14}C_{bulk}$ values do not show any depletion downcore (Figure 2), in agreement with sediment reworking, maybe due to the presence of macrophyte roots in the sediment. Ferguson (1990) determined a sedimentation rate of 0.2 cm year^{-1} for MD-1 using the ^{137}Cs peak and sedimentation plates deployed in the lake for a year. We used this sedimentation rate to determine the possible position of the ^{137}Cs peak in our core (taken 22 years later, Figure S1) and established the age model assuming a constant sedimentation for the upper 40 cm. Below 40 cm, the presence of the organic-rich layer indicates a change in the hydrological regime and sedimentation. The calibrated ^{14}C age for the wood fragment recovered from a core-depth of 45 cm in MD-1 was 1,444 ± 40 C.E. The age at 40 cm calculated with sedimentation rate is 1810 C.E., significantly younger than the wood debris, which, as for the other lakes, likely indicates preaging prior to deposition.

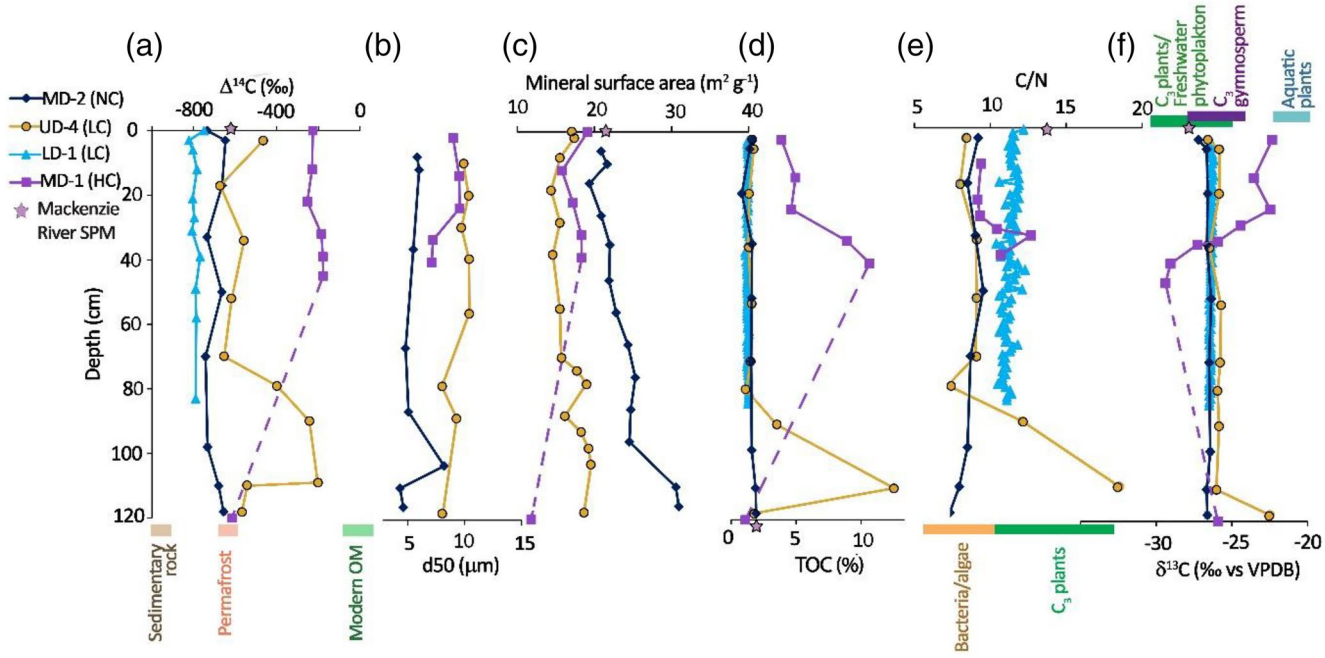

Figure 2. Bulk sediment characteristic with depth in the cores: (a) $\Delta^{14}C_{bulk}$, (b) median grain size (d50), (c) mineral surface area, (d) TOC, (e) C/N_{bulk}, and (f) $\delta^{13}C_{bulk}$. LD-1 data (low closure, Vonk et al., 2016) are plotted for comparison when available, Mackenzie River suspended particulate matter (SPM) is from Vonk et al. (2015b), Holmes et al. (2020) and Goñi et al. (2005). C/N and $\delta^{13}C$ ranges are from Meyers (1994), with the exception of the $\delta^{13}C$ of Mackenzie Delta lake aquatic plants from Tank (2009).

3.2. Bulk and Sedimentological Properties

No-Closure (NC) lake core MD-2: The upper 100 cm of the core from MD-2 (total length, 188 cm, all cores were studied within the topmost 120 cm) has visually distinct laminations with alternating coarser and finer laminae, while below 100 cm there is no evident laminae (Figure S1). The median grain size (d50) varies from 6.0 to 4.3 μm with a downcore decrease linked to an increase in the finer (<2 μm) clay fraction (Figure 2). MSA varies from 19 to 30 m^2g^{-1} with a significant increase in MSA with increasing sediment depth (Figure 2). MSA is inversely correlated with grain size ($r = 0.90$, $p = 0.005$, $n = 6$), as is commonly observed in other rivers and in fluvially dominated sediments (Freymond et al., 2018). The radiocarbon content of the bulk OM ($\Delta^{14}C_{bulk}$) is constant over the core with an average $\Delta^{14}C_{bulk}$ value of −693 ± 40‰ (SD, $n = 9$, core-top value is from Vonk, Giosan et al., 2015). The radiocarbon content of a woody fragment ($\Delta^{14}C_{wood}$) at 157 cm depth is substantially ^{14}C-enriched (−206 ± 66‰), compared to bulk OM. The TOC content and stable carbon isotopic composition of the bulk OM ($\delta^{13}C_{bulk}$) are fairly constant throughout the core, averaging 1.6 ± 0.2% and −26.6 ± 0.4‰, respectively. C/N varies from 7.3 to 9.5, overall constant in the core. εNd is homogenous in the core (−13.36 ± 0.07, 1 SD, $n = 5$, S1).

Low Closure (LC) lake core UD-4: The core (147 cm long) is dominated by clay with organic clasts and no apparent laminae, although there is an organic-rich layer at 107–112 cm (Figure S1). d50 varies between 8.0 and 10.4 μm with finer particles more prevalent toward the bottom of the core, while MSA varies from 14 to 19 m^2g^{-1}, with a steep increase below 70 cm (Figure 2). MSA and d50 are significantly correlated ($r = 0.84$, $p < 0.05$, $n = 8$). $\Delta^{14}C_{bulk}$ values are relatively constant (average of −577 ± 71‰), excluding significantly higher values between 79 and 110 cm (−311 ± 113‰, $n = 3$). One wood fragment at 109 cm—within the ^{14}C-enriched layer—yielded a $\Delta^{14}C_{wood}$ of −203 ± 63‰. TOC contents are relatively constant in the upper section of the core (0–90 cm) and in the deepest sample (av. 1.5 ± 0.2%), but are higher between 90 and 110 cm (max. at 110 cm 12.54%). $\delta^{13}C_{bulk}$ values are relatively uniform throughout the core at −26.0 ± 0.4‰, with the exception of a higher $\delta^{13}C$ value at 118 cm (−22.5 ± 1‰). C/N varies from 7.2 to 18.5, with higher values between 90 and 110 cm. εNd is also homogenous in UD-4 and identical to the composition observed in MD-2 (−13.37 ± 0.11, 1 SD, $n = 6$, Table S1).

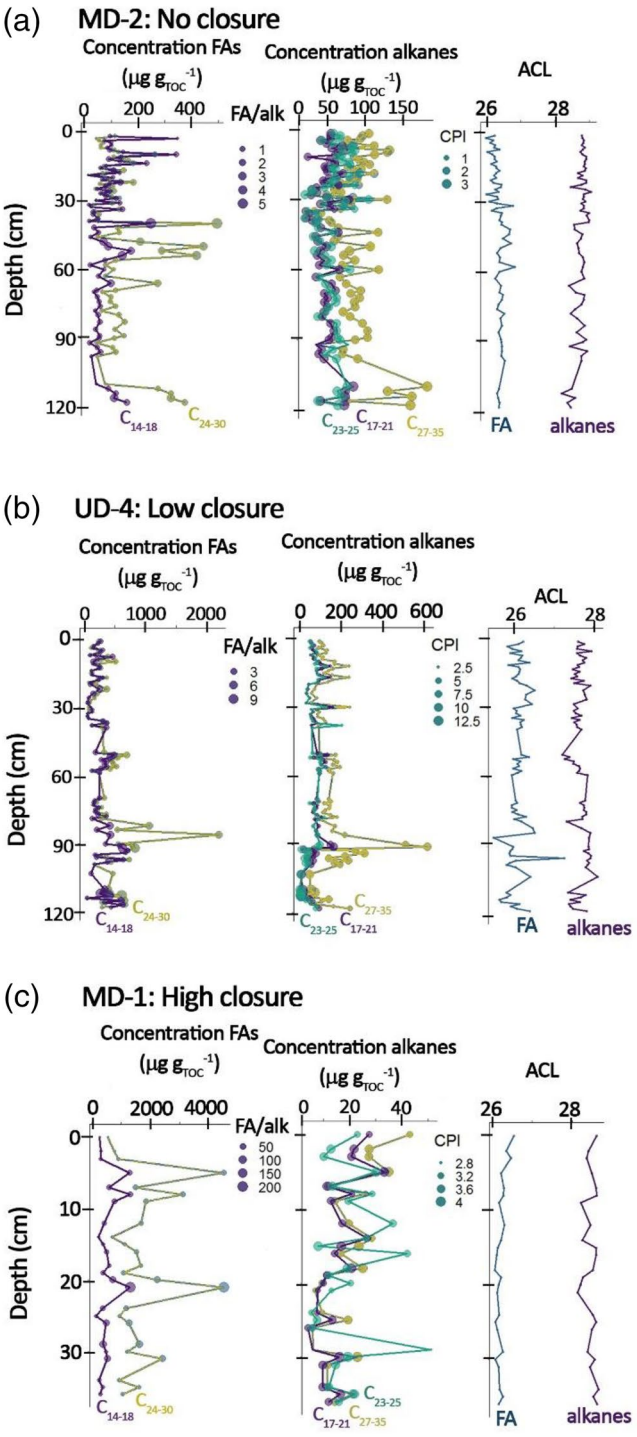

Figure 3. Lipid properties for (a) MD-2 (no closure), (b) UD-4 (low closure) and (c) MD−1 (high closure). First panel: Fatty acid concentration (short-chain C_{14-18} and long-chain C_{24-30}). Symbol sizes reflect the ratio of long-chain FA over long-chain *n*-alkanes as indicated beside each figure. Second panel: *n*-alkanes concentration (short-chain C_{17-21}, mid-chain C_{23-25}, and long-chain C_{27-35}). The symbol sizes reflect the CPI of the *n*-alkanes. Third panel: ACL for FA and *n*-alkanes (blue line for the FA and purple line for the *n*-alkanes). Note the different *x*-axis for all panels. ACL, average chain length; CPI, Carbon Preference Index; FA, fatty acids.

High-Closure (HC) lake core MD-1: The upper 41 cm of core MD−1 (total length 120 cm) is a mix of clay and silt with no apparent laminae that is underlain by a detritus-rich bed (mainly woody debris) at 41–98 cm, hereafter called the peat layer. Beneath 98 cm, the sediment is again a silt/clay mix exhibiting lighter color than the upper 41 cm (Figure S1). d50 varied from 7.1 to 9.5 μm with a downcore decrease (Figure 2) linked to an increase in the finer (<2 μm) clay fraction. MSA varies from 15 to 19 m^2g^{-1} above the peat layer, while it is lower (~12 m^2g^{-1}) below the peat layer (Figure 2). No significant correlation is apparent between d50 and MSA ($r = 0.5$, $p = 0.3$, $n = 5$). $\Delta^{14}C_{bulk}$ is relatively constant above the peat layer (average of −202 ± 37‰, $n = 5$), but is much more ^{14}C-depleted underneath (−615 ± 7‰), the latter $\Delta^{14}C_{bulk}$ values being similar to those of UD-4 and MD-2. One wood fragment retrieved from within the peat layer (45 cm) yielded a $\Delta^{14}C_{wood}$ value of −177 ± 70‰; similar to the $\Delta^{14}C_{bulk}$ values above the peat layer. TOC contents increase with increasing depth starting at 3.9% at the surface to 10.6% at 39 cm, while TOC contents of sediment layers below the peat interval are comparatively low (~1.1%), but similar to those for MD-2 and UD-4. Corresponding $\delta^{13}C_{bulk}$ values decreased with increasing depth, ranging from −22.3 ± 0.15‰ at the top to −29.5 ± 0.15‰ at 39 cm, while the sample below the peat layer has $\delta^{13}C$ value of −25.9 ± 0.15‰ (Figure 2), again echoing typical values in MD-2 and UD-4. C/N varies from 9.1 to 12.7, higher below 30 cm. εNd is homogenous also within much of MD-1 (−13.18 ± 0.08, 1 SD, $n = 4$, Table S1), but slightly more radiogenic than in the other cores (averaging at −13.36 and −13.37, see above). The deepest measured sample at is 120 cm is, however, distinctly unradiogenic (−13.73). Only the upper 41 cm of this core has been studied for lipids due to our focus on the most recent sedimentation and to derive comparisons with MD-2 and UD-4.

3.3. Lipid Distribution and Isotopes

3.3.1. No Closure (MD-2)

n-Alkanes: Chain lengths from C_{17} to C_{35} are detected with the C_{27} *n*-alkane as the dominant homolog (13 ± 3% of all *n*-alkanes C_{17}–C_{35}, $n = 69$) followed by the C_{25} and C_{29} (9 ± 1% for both, $n = 69$). The average CPI is 2.3 ± 0.4, and the ACL is 28.8 ± 0.2 (Figure 3). Average concentrations of the odd short-chain (C_{17-21}), mid-chain (C_{23-25}), and the long-chain (C_{27-33}) *n*-alkanes are 52 ± 14 μg g_{TOC}^{-1}, 47 ± 14 μg g_{TOC}^{-1}, and 87 ± 33 μg g_{TOC}^{-1}, respectively. These concentrations are relatively constant throughout the core with the exception of the long-chain (C_{27-33}) *n*-alkanes, which are higher toward the bottom of the core (up to 183 μg g_{TOC}^{-1} around 110 cm, i.e., 1920 C.E.). There is a slight increase toward the top of the core, above 37 cm (i.e., after 1975 C.E.) in all *n*-alkanes (Figure 3). The mineral surface area-normalized loadings of the *n*-alkanes are significantly correlated with their concentrations ($r = 0.9$ and $p < 0.001$ for all *n*-alkanes). These loadings are also relatively stable over the core but increase above 37 cm (after 1975 C.E.) with long-chain *n*-alkane increasing (C_{27-33}) from 0.03 to 0.08 μgm^{-2}, similar to the mid-chain (C_{23-25}) and short-chain (C_{17-21}) *n*-alkanes increasing from 0.02 to 0.04 μgm^{-2}. The abundance-weighted average $\delta^{13}C$ value of the long-chain (C_{27-33}) *n*-alkanes is −31.4 ± 0.8‰ (Figure 4a). Mid-chain (C_{23-25}) *n*-alkane and C_{21} *n*-alkane $\delta^{13}C$ signatures are identical within uncertainty in all analyzed samples (−30.8 ± 1.6‰, and −30.8 ± 0.5‰, respectively).

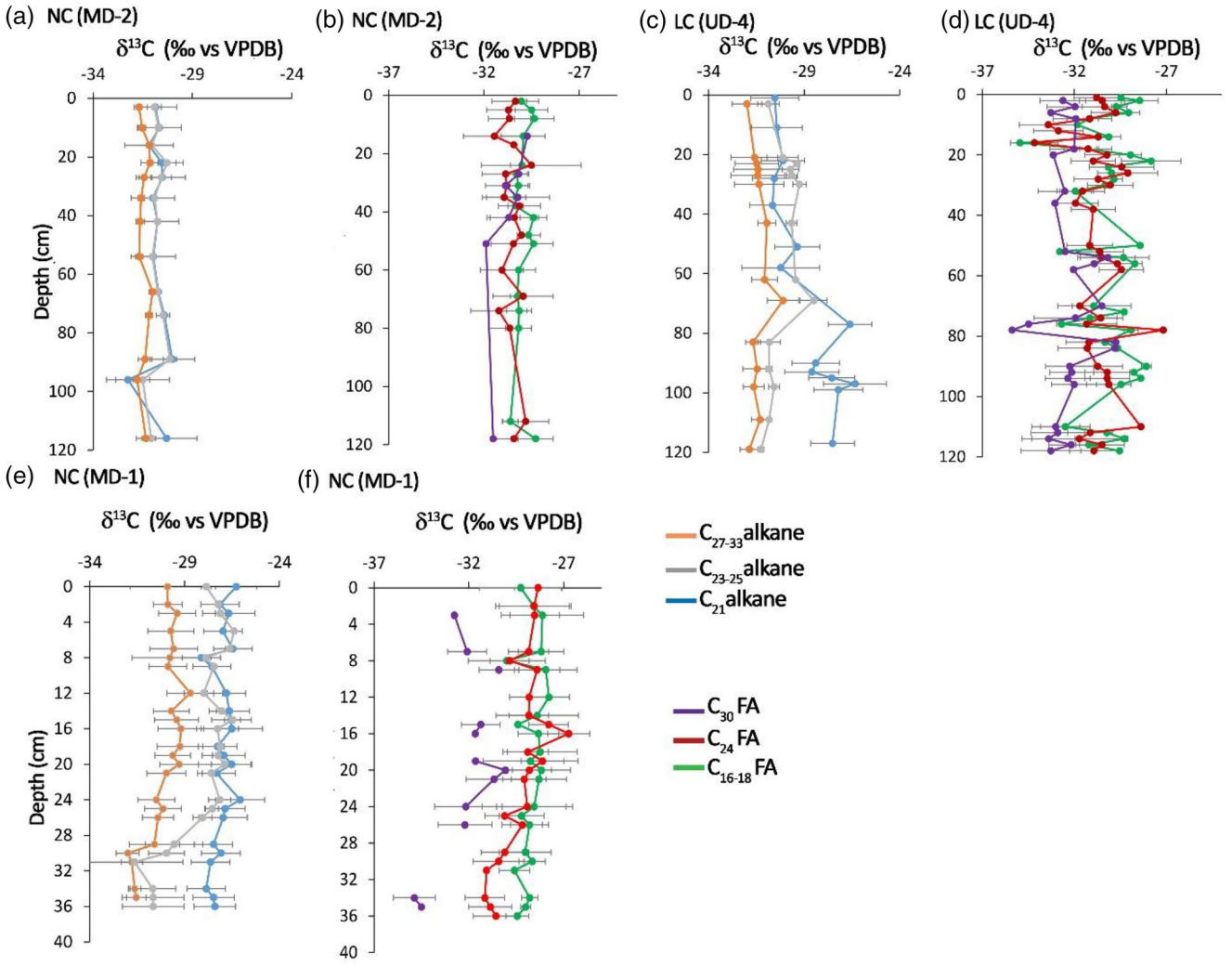

Figure 4. Carbon stable isotope compositions of the *n*-alkanes of (a) MD-2, (c) UD-4, (e) MD-1 and of the fatty acids (FA) of (b) MD-2, (d) UD-4, and (f) MD-1. The error bars represent the variability of the external standard plus the standard deviation among the replicate ($n = 2$) and the effect of added methyl group for the fatty acids.

Fatty (n-alkanoic) acids (FAs): The C_{16} FA is the dominant homolog (21 ± 9% of all FAs, $n = 69$), followed by the C_{24} FA (16 ± 3%, $n = 69$) and C_{22} FA (11 ± 2%, $n = 69$). The summed concentration of the short-chain FAs ($C_{14–18}$) is lower than the long-chain ($C_{24–30}$) counterparts, and decreases from the bottom of the core up to 110 cm (i.e., until 1920 C.E., Figure 3a). It then stays constant at around 125 μg g_{TOC}^{-1} and 83 μg g_{TOC}^{-1} (for the long-chain and short chain FAs, respectively) up to 60 cm (i.e., 1960 C.E.) where all FAs increase. Between 0 and 37 cm (i.e., after 1975 C.E.), the concentrations of the short-chain FAs increase from 30 to 93 μg g_{TOC}^{-1}, with peaks of 340 μg g_{TOC}^{-1} at 3 and 10 cm). The long-chain FAs do not increase during that period, remaining constant at ~60 μg g_{TOC}^{-1}. The mineral surface area-normalized loadings of the FAs show the same trend as the concentrations ($r > 0.9$, $p < 0.001$). The weighted average $\delta^{13}C$ value of the short chain FAs ($C_{16–18}$) is −30.0 ± 3.1‰ ($n = 19$), the $\delta^{13}C$ value of the C_{24} FA is similar (−30.5 ± 0.5‰, $n = 19$), but the C_{30} homolog could only be sporadically measured (−30.7 ± 0.7‰, $n = 6$, Figure 4b). The $\delta^{13}C_{C30\ FA}$ value is lower at the bottom of the core and increases toward the top.

3.3.2. Low Closure (UD-4)

n-Alkanes: The most abundant *n*-alkane throughout the core is the C_{27} homolog (19 ± 1%, $n = 76$), followed by *n*-C_{25} (10 ± 1%, $n = 76$) and *n*-C_{29} (8 ± 1%, $n = 76$). The average CPI is 4.0 ± 2.6, however, there is a clear separation between the 90–110 cm section of the core (CPI of 8.6 ± 2.4) and the rest of the core (0–86 and 111–118 cm; CPI of 2.9 ± 0.5; significant difference *t*-test $p < 0.0001$, Figure 3b). The ACL, on the other hand, is similar throughout the core: 90–110 cm at 27.8 ± 0.2 and the rest at 27.6 ± 0.2. The concentration of the long-chain ($C_{27–33}$) *n*-alkanes is higher for the 90–110 cm layer (236 ± 175 μg g_{TOC}^{-1}; max. 614 μg g_{TOC}^{-1} at 90 cm), whereas the short-chain ($C_{17–21}$) and mid-chain ($C_{23–25}$) *n*-alkanes are lower than in the rest of the core (32 ± 28 and 64 ± 48 μg g_{TOC}^{-1}). The long-chain *n*-alkane loadings are also higher in this layer (0.4 ± 0.2 μgm^{-2}). In the rest of the core, long-chain, mid-chain and short-chain *n*-alkane concentrations are relatively constant (131 ± 46 μg g_{TOC}^{-1}, 79 ± 27 μg g_{TOC}^{-1} and 76 ± 28 μg g_{TOC}^{-1}, respectively). The *n*-alkane loadings are significantly correlated with their concentrations ($r = 0.9$, $r = 0.7$ and $r = 0.7$, $p < 0.001$ for the short-chain, mid-chain and long-chain *n*-alkanes, respectively), with similar loadings for all *n*-alkanes (short-chain: 0.07 ± 0.03 μgm^{-2}, mid-chain 0.07 ± 0.03 μgm^{-2}, and long-chain: 0.12 ± 0.05 μgm^{-2}). The average $\delta^{13}C$ value of the C_{21} *n*-alkane is −28.9 ± 1.6‰, while the abundance-weighted average $\delta^{13}C$ values of the mid-chain (C_{23} – C_{25}) and the long-chain (C_{27}–C_{33}) *n*-alkanes are −29.8 ± 0.5‰ and −31.4 ± 3.4‰, respectively Figure 4c). The $\delta^{13}C$ value of the C_{21} *n*-alkane is lower below 80 cm than above (∼−30.5‰ compared with ∼−27.5‰).

FAs: The main *n*-FA homolog is C_{16} (24 ± 5%, $n = 76$) followed by C_{24} (17 ± 4%, $n = 76$) and C_{22} (13 ± 2%, $n = 76$). The concentration of the short- and long-chain FAs is different between the two layers mentioned above (*t*-test $p < 0.0001$): 392 ± 201 μg g_{TOC}^{-1} ($C_{14–18}$) and 510 ± 210 μg g_{TOC}^{-1} ($C_{24–30}$, $n = 16$) for the 90–110 cm layer, versus 228 ± 131 μg g_{TOC}^{-1} ($C_{14–18}$) and 260 ± 160 μg g_{TOC}^{-1} ($C_{24–30}$, $n = 60$) in the rest of the core (Figure 3b). Corresponding loadings of the FAs are higher for the 90–110 cm layer (1.5 ± 1 μgm^{-2}) than the rest of the core (0.2 ± 0.1 μgm^{-2}). The correlation between FA concentration and mineral loading is significant but lower than for the *n*-alkanes ($r = 0.6$ and $p < 0.001$). The abundance-weighted average of the $\delta^{13}C$ values of the short-chain FAs ($C_{16–18}$) is −30.1 ± 1.5‰, similar to the values of the C_{24} FA (av. −30.7 ± 1.2‰), while the C_{30} homolog is slightly more ^{13}C-depleted (av. of −32.3 ± 1.2‰, Figure 4). There is a slight increase in $C_{30\ FA}$ $\delta^{13}C$ values from the bottom of the core up to 80 cm before sharply decreasing (to −35‰ at 80 cm) and a further decrease toward the top of the core (−2‰). The $\delta^{13}C_{C24\ FA}$ and $\delta^{13}C_{C16–18\ FA}$ values are highly variable at the bottom of the core but show two episodes of ^{13}C-enrichment at the top of the core (+2‰ and +4‰ at 32 cm for the C_{24} and $C_{16–18}$, respectively, and +4‰ at 10 cm for both).

3.3.3. High Closure (MD-1)

n-Alkanes: The C_{27} homolog is the dominant *n*-alkane (14 ± 2%, $n = 24$), followed by *n*-C_{23} (13 ± 2%, $n = 24$) and *n*-C_{25} (8 ± 2%, $n = 24$). The ACL and CPI values are 28.5 ± 0.1 and 3.5 ± 0.3, respectively (Figure 3c). Concentrations of the short- mid and long-chain alkanes are similar and relatively stable throughout the core (∼20 μg g_{TOC}^{-1}), but much lower than for MD-2 and UD-4. The mineral surface area-normalized loadings of the long-, mid and short-chain *n*-alkanes are relatively constant over the core (average of 0.06 ± 0.03 μgm^{-2}, 0.05 ± 0.02 μgm^{-2}, and 0.07 ± 0.05 μgm^{-2}, respectively), and correlated with *n*-alkane concentrations ($r = 0.8$, $r = 0.6$, $r = 0.6$, $p < 0.001$, for the short-chain, mid-chain, and long-chain homologs, respectively). The $\delta^{13}C$ values of odd-carbon-numbered *n*-alkanes are higher for *n*-C_{21} (−27.0 ± 0.5‰, $n = 24$) than for the $C_{23–25}$ and $C_{27–33}$ homologs (−28.1 ± 4.7‰ and −30.1 ± 4.6‰, respectively, $n = 24$, Figure 4e). There is an increase in the $\delta^{13}C$ values of the mid-chain *n*-alkanes between 32 and 24 cm (from −30.7 to −26.4‰).

FAs: The dominant *n*-FA is the C_{26} homolog (24 ± 2%, $n = 24$) followed by C_{24} (20 ± 2%, $n = 24$) and C_{28} (16 ± 2%, $n = 24$). Concentrations of long-chain ($C_{24–30}$) FAs are much higher than short-chain ($C_{14–16}$) FAs (1,648 ± 1,052 μg g_{TOC}^{-1} and 512 ± 333 μg g_{TOC}^{-1}, respectively), and are up to 30 times higher than in MD-2 and 6 times higher than in UD-4 (Figure 3c). This suggests a higher degree of preservation as suggested by the higher ratio of long-chain FAs over long-chain *n*-alkanes (5–200, $n = 24$) and higher CPI (Figure 3c). The concentration profile of the long-chain FA exhibits two peaks, one at 20 cm (4,495 μg g_{TOC}^{-1}) and one at 5 cm (5,000 μg g_{TOC}^{-1}), whereas the short-chain FAs only shows moderate peaks for the same periods (1,292 and 1,264 μg g_{TOC}^{-1} at 20 and 5 cm, respectively). Corresponding FA loadings are strongly correlated with

the concentrations ($r = 0.8$, $p < 0.001$) throughout the core, with slightly higher mineral loadings (as high as 12 μgm^{-2}) between 5–10 cm, 20–25 cm and 30–35 cm, yet no systematic trend with depth. The average $\delta^{13}C$ values for the C_{16-18} FAs are higher (−28.7 ± 1.8‰, $n = 24$) compared to the C_{24} and C_{30} FAs (−29.2 ± 1.1‰ and −31.7 ± 1.9‰, respectively, Figure 4f). The $\delta^{13}C$ values of the C_{30} FA increases over the core (from −34 to −32‰).

4. Discussion

4.1. Sedimentary History of the Lakes

From low closure to no closure (MD-2): There are some major discontinuities in the studied sediment cores, highlighting changes in the hydrological regime of the lakes (Figure S1). As noted by Vonk et al. (2016), the presence of well-defined laminations corresponding to deposition since 1932 C.E. in core MD-2 indicates that it has been a no-closure lake during this time period. However, before 1932 C.E., MD-2 was low closure (Vonk et al., 2016) and prior to that, it had likely been dry (as indicated by the presence of a peat layer at 157 cm). The transition from low closure to no closure (last ∼ 90 years, transition at around 100 cm) is accompanied by several changes in the sedimentary properties, including a decrease in MSA and a sharp increase in d50 just before the transition, as well as a small decrease in $\Delta^{14}C_{bulk}$, TOC content (Figure 2) and also in alkane CPI values (Figure 3). But there are no associated changes in εNd, indicating no major variation in the mineral source (Table S1). In the low closure state, there are proportionally more long-chain alkanes and long-chain FAs in comparison to the short-chain homologs. This enhanced abundance of short-chain alkanes during no closure can be related to increased inputs of short-chain petrogenic alkanes delivered by the Mackenzie River, which also leads to the (subtle) decrease in $\Delta^{14}C_{bulk}$ and a drop in CPI (Figures 2 and 3), while higher concentration of long-chain FA in the low closure state may reflect enhanced preservation (higher CPI, TOC) due to longer periods of water column anoxia.

From high closure to low closure (UD-4): Core UD-4 has an organic-rich layer (TOC > 2%) from 110 to 94 cm indicating a possible transition from HC to LC at around 1890 C.E. This transition is accompanied by a large decrease in $\Delta^{14}C_{bulk}$, as well as in TOC, C/N ratios (Figure 2) but also CPI of *n*-alkanes (Figure 3), the latter suggesting proportionally greater petrogenic input in the low closure state. The MSA was generally higher during the high than the low closure state (although no clear grain size difference is noted, Figure 2), however this observation might be due to the creation of ash (with high MSA > 50 m^2g^{-1}; e.g., Downie et al., 2009) after combustion of organic-rich sediments during preparation of the samples (Wakeham et al., 2009). $\delta^{13}C_{bulk}$ was invariant over this transition (with the exception of a high value, −22.5‰, well before the transition, Figure 2). The peak in long-chain alkane and FA concentrations just after this period (Figure 3) suggests enhanced terrestrial input from the Mackenzie River, possibly triggered by a stronger spring freshet that reduced the height of the levee of UD-4, transforming it into a LC lake. The constant values of εNd (Table S1) indicate that this change of connection is not accompanied by a change in source rock and that the Mackenzie River remained the dominant sediment source.

From no closure to dry to high closure (MD-1): Core MD-1 core presents two discontinuities, one at 95 cm (from homogeneous silt/clay to organic-rich sediment with large plant debris), and the other one at 44 cm returning back to a mix of silt and clay (with some rare plant debris, Figure S1). The first discontinuity possibly reflects the transition from a NC state to a drier state, creating a peat layer. TOC, $\delta^{13}C_{bulk}$ and $\Delta^{14}C_{bulk}$ values below 95 cm are similar to those of present-day MD-2 (NC), while the MSA is lower than in MD-2 (Figure 2). The εNd observed at 120 cm is clearly less radiogenic than further above the peat layer, which might indicate more input from the Mackenzie River (Table S1). The peat layer likely represent a period of time when MD-1 did not receive any water (and thus sediments, OC, nutrients etc.) from the Mackenzie River, with lacustrine sedimentation commencing again at 45-40 cm maybe due to sea-level rise (Lesack & Marsh, 2007). MSA, TOC, $\Delta^{14}C_{bulk}$, and $\delta^{13}C_{bulk}$ values increase (Figure 2), there is a high proportion of long-chain FA relatively to short-chain FA but not more long-chain alkanes than short-chain alkanes (Figures 3 and 5). There are no further distinct changes until the top of the core, hence we assume a constant hydrological connection to the river during that time, that is, it has remained in high closure state.

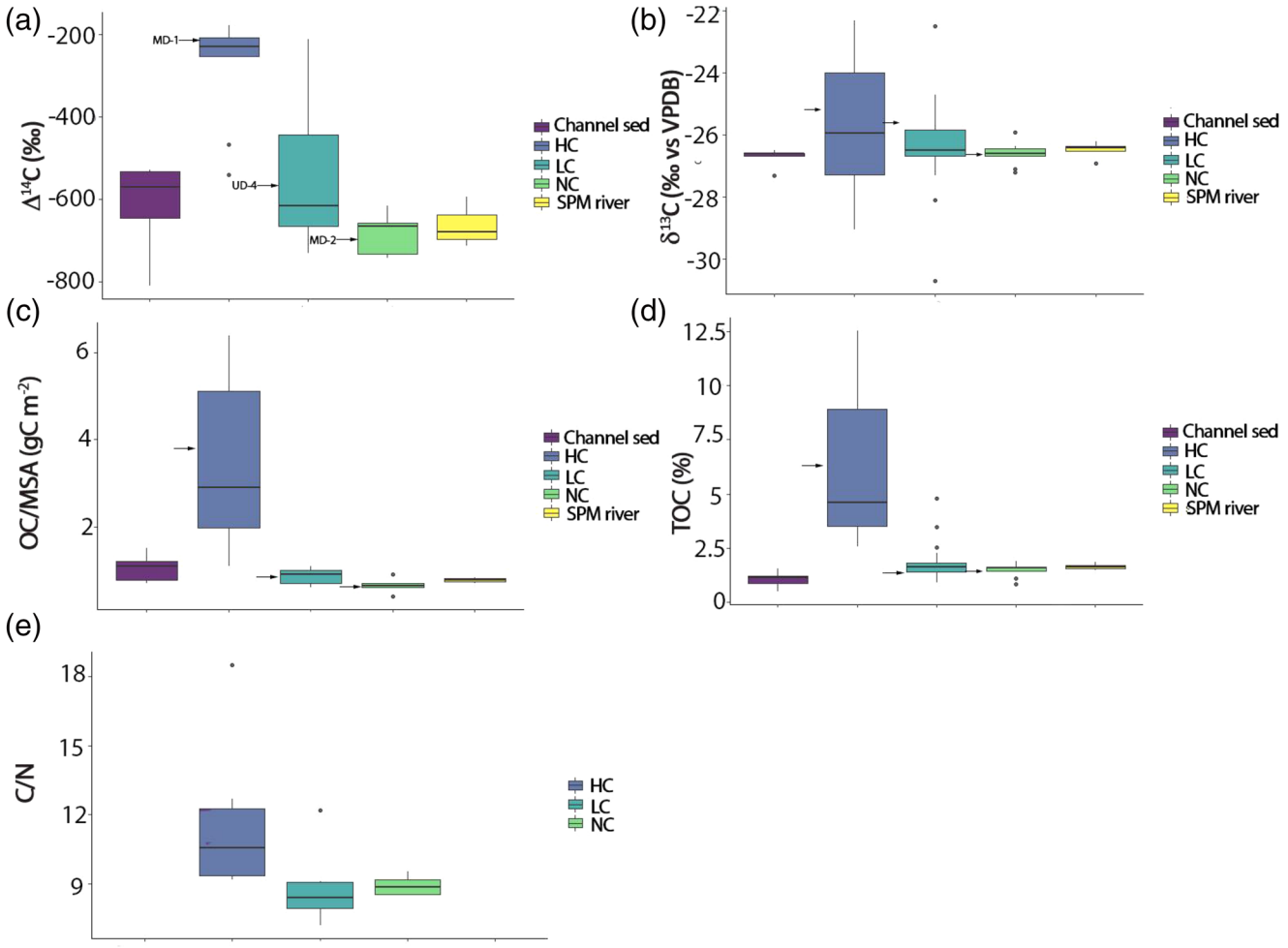

Figure 5. Bulk characteristics of HC, LC, and NC lakes (our study and Vonk, Giosan et al., 2015) (a) $\Delta^{14}C$, (b) $\delta^{13}C$, (c) organic carbon (OC) loadings: mineral surface area (MSA), (d) TOC, and (e) C/N ratios (values are only from the three studied lakes). Mackenzie River SPM and channel sediments (Vonk, Giosan et al., 2015) are plotted when available. The arrows represent the average values for the three studied lakes (MD-1 for HC, UD-4 for LC and MD-2 for NC). HC, High-closure; LC, Low-closure; NC, No-closure; SPM, Suspended particulate matter; TOC, Total sediment OC.

Based on the above observations, several common sedimentological and geochemical features emerge with respect to transitions in lake connectivity. Transition from NC to LC to HC is accompanied by increases in MSA, TOC, and $\Delta^{14}C_{bulk}$, likely due to less petrogenic input originating from the river as well as an increase in macrophyte production. There are also changes at the molecular level (e.g., higher *n*-alkane CPI and higher long-chain FA concentrations) which point toward more production and better preservation of fresh OC in high closure state (further discussed in Section 4.2), with the largest changes recorded when a lake transitions from LC to HC and vice-versa (Figure 5). Similarly, significant changes in $\delta^{13}C_{bulk}$ are only apparent for the transition between LC and HC, indicating a significant change in the source of OM deposited in the lake, likely due to the increase in macrophyte production (Figure 5). The LC and NC states seem to be very similar in term of sedimentary and bulk OC properties but also on a molecular level, reflecting the dominance of Mackenzie River sediment and OM supply during these degrees of connectivity. The underlying processes responsible for these changes are discussed in the subsequent sections.

4.2. Organic Matter Deposition in the Mackenzie Delta Lakes

4.2.1. Carbon Source

High closure: Of the three lakes, HC lake MD-1 sediments return the highest $\Delta^{14}C_{bulk}$ values (−202 ± 37‰ above 40 cm), and correspondingly young radiocarbon ages (1893 ± 325 ^{14}C year). Similarly, UD-4 has relatively ^{14}C-enriched "younger" bulk OC ($\Delta^{14}C_{bulk} > -400$‰) during high closure state (90–110 cm) with a similar ^{14}C age as the woody debris present in this layer. During high closure state, preaged carbon is seldom introduced from the river during the freshet (Marsh & Hey, 1994), and the sediments reflect inputs from the surrounding vegetation and soils, as well as from aquatic in situ productivity (vary variable $\delta^{13}C_{bulk}$ but constant $\Delta^{14}C_{bulk}$, Figure 5). Marsh and Hey (1994) observed that MD-1 has 55% chance of not being flooded each year, due to its elevation (i.e., 4.1 m.a.s.l.), with the impact of flooding being limited in extent. For example, MD-1 received 50 mgL^{-1} sediment from the river in 1987 while nearby no closure lakes received 500 mgL^{-1} (Ferguson, 1990). Correspondingly, OC deposition in high closure lakes is dominated by autochthonous inputs.

Low and no closure: Core UD-4 bulk OC $\Delta^{14}C$ values (−577 ± 17‰) are similar to those of the bank sediment and suspended particulate matter (SPM) from the Mackenzie River in June, that is, during the freshet (−529 ± 12‰ and −615 ± 70‰, respectively, Holmes et al., 2020; Vonk, Giosan et al., 2015), suggesting that the OC in sediments deposited in the lake is predominantly derived from riverine suspended sediments (Figures 2 and 5). This is consistent with the dynamics of LC lake, where the spring freshet inundates the lake river with sediment-laden waters. UD-4 does not show a great influence of modern OC and there is no documentation on macrophyte cover for this lake. Similar observations can be made for MD-2, where the bulk $\Delta^{14}C$ values of OC (−695 ± 38‰) agree with those reported for Mackenzie river SPM (−615 ± 70‰, Holmes et al., 2020; Vonk, Giosan et al., 2015).

4.2.2. Influence of Petrogenic Input on LC and NC Lakes

To calculate the influence of petrogenic OC in NC and LC lakes, Vonk et al. (2015b) defined a binary mixing model using $\Delta^{14}C$ (Equation 5) and (Equation 6):

$$\Delta^{14}C_{petro} \times F_{petro} + \Delta^{14}C_{biogenic} \times F_{biogenic} = \Delta^{14}C_{sample} \quad (5)$$

$$F_{petro} + F_{biogenic} = 1 \quad (6)$$

Adopting end-member values for $\Delta^{14}C_{petro} = -1000$‰ and $\Delta^{14}C_{biogenic} = -501 \pm 186$‰ (representing significantly preaged biogenic carbon, Hilton et al., 2015; Vonk, Giosan et al., 2015), LC (UD-4) and NC (MD-2) have a different petrogenic contributions (17%–29% and 38%–47%, respectively). Consistent with expectations, LC lake, has a lower petrogenic hydrocarbon influence and a higher in situ production than NC lake, the latter being constantly connected to the Mackenzie River.

No closure lake (MD-2): The high concentration of the short-chain *n*-alkanes (160 μg g_{TOC}^{-1}, C_{17} to C_{25}, in comparison with the long-chain 130 μg g_{TOC}^{-1}, Figure 3) suggests inputs from fossil hydrocarbons derived from sedimentary rocks, which are common in the Mackenzie drainage basin (Drenzek et al., 2007; Goñi et al., 2005; Hilton et al., 2015; Tolosa et al., 2013; Yunker et al., 2002) This is confirmed by the low CPI (Figure 5), on average 2.3 ± 0.4 (>5 on average for extant higher plants, ~1 for petroleum *n*-alkanes, Collister et al., 1994). This average CPI value is similar to that reported for the Mackenzie River itself (CPI = 2.35, Tolosa et al., 2013) where about 17%–50% of the *n*-alkanes in SPM originate from a petrogenic source (calculated following [Equation 5] and [Equation 6], and using data of Hilton et al., 2015). Furthermore, the $\delta^{13}C$ values of all odd *n*-alkanes (C_{21-31}) are invariant, centered around −31.3 ± 0.8‰, similar to the $\delta^{13}C$ of the C_{22} *n*-alkane (−31.2‰) (Figure 4), assumed to be totally petrogenic (Hilton et al., 2015). Using the binary model (Equations 5 and 6), the proportion of petrogenic hydrocarbons over all *n*-alkanes can be determined (38–47% for NC MD-2) and the biogenic $\delta^{13}C$ values can be derived as follows (Equation 7):

$$\delta^{13}C_{petro} \times F_{petro} + \delta^{13}C_{biogenic} \times F_{biogenic} = \delta^{13}C_{sample} \quad (7)$$

With $\delta^{13}C_{petro} = \delta^{13}C_{c22\ alkane} = -31.2‰$.

The calculated biogenic $\delta^{13}C$ of the long-chain (C_{27}–C_{33}) *n*-alkanes varies from −30.5 to −32.9‰, overlapping with the petrogenic value. In NC MD-2, ACL (28.8 ± 0.2) and $\delta^{13}C_{biogenic}$ of the long-chain *n*-alkanes are in agreement with C_3 vegetation classically found in high latitude catchment (Collister et al., 1994; Diefendorf & Freimuth, 2017). The long-chain FAs are also in agreement with a C_3-dominated, input with a dominant C_{24} FA and $\delta^{13}C$ of −30.6 ± 2.4‰, similar values for long-chain FA report (−35 to −31‰) in Mackenzie river SPM reported by Goñi et al. (2005) and Tolosa et al. (2013). Although the dominant FA in river SPM is the *n*-C_{26} (Vonk et al., 2016), MD-2 *n*-alkanes and FAs appear to primarily reflect OM transported by the river.

Low closure lake (UD-4): In comparison to the no-closure setting of NC lake (MD-2), LC lake (UD-4) has a lower petrogenic carbon influence and a higher CPI (2.8 ± 0.3, Figure 3) which may indicate local organic matter input to the lake. The $\delta^{13}C$ values of the long-chain *n*-alkanes (corrected for the influence of the petrogenic hydrocarbons using $\delta^{13}C_{C22\ alkane} = -30.7 \pm 0.7‰$, Figure 4) is −33.3 ± 0.7‰ for the *n*-C_{33} homolog, which suggests a mixed angiosperm/gymnosperm (coniferous) OC source. For the $C_{29–31}$, $\delta^{13}C$ values (−31.4 ± 0.3‰) are similar to the C_{22} homolog, while $\delta^{13}C$ values of C_{21} to C_{25} *n*-alkanes are consistent with higher plant inputs (−28.5 to −30.5‰, Chikaraishi & Naraoka, 2005).

4.2.3. Burial Efficiency and Carbon Fluxes in the Mackenzie Delta Lake Sediments

Factors such as oxygen availability, solid iron phases, type, and specific surface area of minerals as well as particle size have been suggested to control the preservation and burial efficiency of organic matter in lakes, rivers, and oceans (Blattmann et al., 2019; Galy et al., 2008; Hemingway et al., 2017; Keil et al., 1997; Lalonde et al., 2012, Sobek et al., 2009). The association of OM with mineral surfaces has been inferred to play a key role based on a positive correlations between MSA and TOC in sediments (Galy et al., 2008; Mayer, 1994), potentially by shielding OM from enzymatic hydrolysis (Burdige, 2007; Mayer, 1994). For all studied lakes, the MSA increased with decreasing d50, as observed in other fluvial systems (Figure S2, Galy et al., 2008; Keil et al., 1997; Mayer, 1994; Tao et al., 2015; Vonk, Giosan et al., 2015). In the Mackenzie Delta, this correlation is governed by variable clay fractions (<4 μm) characterized by high MSA (Vonk, Tank, et al., 2015). For the NC and LC lakes (cores MD-2 and UD-4, TOC < 2%), TOC is also positively correlated with MSA, contrasting with the HC lake (MD-1, Figure 5). The OC loadings (ratio of OC to MSA) are 0.6 ± 0.1 $mg_{OC}\ m^{-2}$ for MD-2, 0.9 ± 0.1 $mg_{OC}\ m^{-2}$ for UD-4, and 3.7 ± 1.6 $mg_{OC}\ m^{-2}$ for MD-1 (Figure 5), while Vonk et al. (2015b) observed an average of 0.8 ± 0.2 $mg_{OC}\ m^{-2}$ for surface sediments of lakes in the Mackenzie River Delta ($n = 11$). Usual loadings for river sediments are between 0.4 and 1.0 $mg_{OC}\ m^{-2}$, with lower values indicative of greater decomposition and higher values indicative of enhanced preservation (Blair & Aller, 2012). Higher loadings are usually found in lake sediments with higher TOC content (e.g., 2.5–15 $mg_{OC}\ m^{-2}$ for TOC > 20%, Sobek et al., 2009), although no correlation between MSA and TOC occurs due to the abundance of discrete organic matter particles or fragments. The lower mineral loadings found in NC (MD-2) and LC (UD-4) and the positive correlation with MSA point toward a "riverine signature," similar to that of the Mackenzie River itself (Mackenzie River SPM OC loading of 0.4 $mg_{OC}\ m^{-2}$, Goñi et al., 2005). In UD-4, during high closure state (90–110 cm), OC loadings of up to 6.4 $mg_{OC}\ m^{-2}$ are present, similar to those of MD-1 (max. 5.8 $mg_{OC}\ m^{-2}$). Here, the absence of a positive correlation between TOC and MSA likely reflects the presence of plant debris not sorbed to mineral surfaces, and more generally, relates to the large supply of organic matter allied with strong preservation. Therefore, another characteristic of high closure lakes seems to be higher OC:MSA ratios indicative of burial of (young) carbon (Figure 5).

Flux: The flux of organic carbon to the sediment over a certain period of time can be calculated following (Equation 8):

$$\mathrm{Flux}_{OC} = D \times R \times TOC \tag{8}$$

With *R* being the sedimentation rate (in cm $year^{-1}$), *D* the bulk density (from Vonk et al., 2015b, bulk density for MD-1 has been taken from Marsh et al., 1999, 0.893 gcm^{-3}) and TOC, the carbon content of the sediments (in gg^{-1}). Marsh et al. (1999) observed large variations in the bulk density of the Mackenzie Delta

lake sediments, highlighting the importance of using a lake-specific sediment densities instead of averages for lakes with the same closure state. Unfortunately, since lake-specific bulk densities are not available for MD-1, our fluxes are averaged following Marsh et al. (1999) and are likely underestimated. Furthermore, due to the limited constraints on the age model, sedimentation rates were calculated linearly from one tie point (1963–1964 C.E., see Section 3.1.) and, hence come with some uncertainty. Accepting these limitations, we find that the area-normalized flux of OC to the sediment is higher in the NC lake (MD-2, 280 ± 104 gCm^{-2} $year^{-1}$ averaged over the core, $n = 9$) than in the LC lake (UD-4, 151 ± 22 gCm^{-2} $year^{-1}$ averaged over the core, $n = 7$) and the HC lake (MD-1, 118 ± 53 gCm^{-2} $year^{-1}$ averaged over the core, $n = 5$). Using their surface area, these fluxes translate to 2,125 × 10^6 gC $year^{-1}$ for MD-2, 22 × 10^6 gC $year^{-1}$ for UD-4, 11 × 10^6 gC $year^{-1}$ for MD-1, in comparison, the three main Alaskan rivers export 297 × 10^6 gC $year^{-1}$ into the Beaufort Sea (Mcclelland et al., 2014). The OC flux per area for another LC lake (LD-1, located in the outer delta, 211 ± 25 gCm^{-2} $year^{-1}$ averaged over the core, $n = 16$, Figure 1) is between the fluxes observed for MD-2 and UD-4. All these values are comparable to observations from lakes in the northern USA (9–318 gCm^{-2} $year^{-1}$, Hobbs et al., 2013). Overall, the median carbon flux encountered in lakes around the world is 40 gCm^{-2} $year^{-1}$ (not counting reservoirs, see Mendonça et al., 2017) is not really representative of the Mackenzie Delta lakes which show a large range of values. The distinctive characteristics of the shallow Mackenzie Delta lake systems, for example, highly productive for HC lakes or high sedimentation rates due to riverine input for NC, coupled to the aerial extent, make these systems a hotspot of OC burial, with sharp contrasts in the provenance of this OC between lake types. With about 45,000 lakes (12% NC, 55% LC and 33% HC, Marsh & Hey, 1989) and a deltaic surface of 13,000 km^2, we estimate a carbon burial of ~2 MtC $year^{-1}$ for the whole delta, similar to the estimate of 1.07 (±4) MtC $year^{-1}$ of Macdonald et al. (1998). Our estimate considers the four mentioned lakes as representative of NC (MD-2), LC (average of UD-4 and LD-1) and HC (MD-1) lakes. Future work should aim at extending these observations. An increase in the aerial extent of HC lakes caused by a decrease in the freshet volume due to global anthropogenic-driven changes could decrease the efficiency of trapping carbon in this region.

5. Conclusions

The Mackenzie River Delta lakes are under a strong ongoing climate change with a rise in sea-level started at the onset of the Holocene and increasing under anthropogenic warming, and a strong increase in winter air temperature. These alterations will influence the lakes' connectivity to the main river and possibly their carbon burial efficiency. The three sediment cores studied reveal that changes in lake to river connectivity are accompanied by striking changes in bulk and molecular properties of the sediment, as a lake's connection decreases (from NC to LC/HC) the sediment become coarser and the mineral surface area decrease. Furthermore the OM buried is "fresher" with higher CPI, C/N and $\Delta^{14}C_{bulk}$, likely due to a larger fraction originating from autochthonous macrophyte productivity. Long-chain fatty acids become more abundant possibly due to stronger or prolonged period of anoxia, while short-chain petrogenic *n*-alkanes supplied by the river are subdued. As such, high closure lakes may record local climatic and hydrologic changes. Low- and no-closure lakes, on the other hand, are strongly impacted by petrogenic carbon originating from the river but have the capacity to bury more carbon. As the Mackenzie Delta lakes may transition to other connection state, that is, decreased connection due to declining effects of river-ice breakup or increased due to rise in sea-level, the burial of carbon in the delta as a whole will change, likely diminishing in efficiency as carbon trap.

Conflict of Interest

The authors declare no conflicts of interest relevant to this study.

Data Availability Statement

All data presented in this article are available (https://doi.org/10.1594/PANGAEA.924201).

Acknowledgments
The authors thank the sampling team that assisted T. I. Eglinton and L. Giosan in collecting the sediment cores from the Mackenzie River lakes and Jorien Vonk and Daniel Montluçon for slicing MD-1 and UD-4. Grain size analysis were performed in the Limnogeology lab at ETH Zurich and radiocarbon and elemental analyses were performed in conjunction with the Laboratory for Ion Beam Facility in ETH Zurich. Carbon isotopes were measured at the Climate Geology Department of the ETH Zurich with the help of Steward Bishop. J. Lattaud was funded by a Rubicon grant (019.183EN.002) from NWO, Netherlands Organization for scientific research.

References

Amon, R. M. W., Rinehart, A. J., Duan, S., Louchouarn, P., Prokushkin, A., Guggenberger, G., et al. (2012). Dissolved organic matter sources in large Arctic rivers. *Geochimica et Cosmochimica Acta*, *94*, 217–237. https://doi.org/10.1016/j.gca.2012.07.015

Aufdenkampe, A. K., Mayorga, E., Raymond, P. A., Melack, J. M., Doney, S. C., Alin, S. R., et al. (2011). Riverine coupling of biogeochemical cycles between land, oceans, and atmosphere. *Frontiers in Ecology and the Environment*, *9*(1), 53–60. https://doi.org/10.1890/100014

Bastviken, D., Tranvik, L. J., Downing, J. A., Crill, P. M., & Enrich-Prast, A. (2011). Freshwater methane emissions offset the continental carbon sink. *Science*, *331*(6013), 50. https://doi.org/10.1126/science.1196808

Battin, T. J., Luyssaert, S., Kaplan, L. A., Aufdenkampe, A. K., Richter, A., & Tranvik, L. J. (2009). The boundless carbon cycle. *Nature Geoscience*, *2*(9), 598–600. https://doi.org/10.1038/ngeo618

Blair, N. E., & Aller, R. C. (2012). The Fate of terrestrial organic carbon in the marine environment. *Annual Review of Marine Science*, *4*(1), 401–423. https://doi.org/10.1146/annurev-marine-120709-142717

Blattmann, T. M., Liu, Z., Zhang, Y., Zhao, Y., Haghipour, N., Montluçon, D. B., et al. (2019). Mineralogical control on the fate of continentally derived organic matter in the ocean. *Science*, *366*(6466), 742–745. https://doi.org/10.1126/science.aax5345

Bray, E., & Evans, E. (1961). Distribution of *n*-paraffins as a clue to recognition of source beds. *Geochimica et Cosmochimica Acta*, *22*, 2–15. https://doi.org/10.1016/0016-7037(61)90069-2

Brunauer, S., Emmett, P. H., & Teller, E. (1938). Adsorption of gases in multimolecular layers. *Journal of American Chemistry Society*, *60*(2), 309–319. https://doi.org/10.1021/ja01269a023

Burdige, D. J. (2007). Preservation of organic matter in marine sediments: Controls, mechanisms, and an imbalance in sediment organic carbon budgets?. *Chemical Reviews*, *107*(2), 467–485. https://doi.org/10.1021/cr050347q

Carson, M. A., Jasper, J. N., & Conly, F. M. (1998). Magnitude and sources of sediment input to the Mackenzie Delta, northwest territories. *Arctic*, *51*(2), 116–124. https://doi.org/10.14430/arctic1053

Chikaraishi, Y., & Naraoka, H. (2005). $\delta^{13}C$ and δD identification of sources of lipid biomarkers in sediments of Lake Haruna (Japan). *Geochimica et Cosmochimica Acta*, *69*(13), 3285–3297. https://doi.org/10.1016/j.gca.2005.02.023

Cole, J. J., Prairie, Y. T., Caraco, N. F., McDowell, W. H., Tranvik, L. J., Striegl, R. G., et al. (2007). Plumbing the global carbon cycle: Integrating inland waters into the terrestrial carbon budget. *Ecosystems*, *10*(1), 171–184. https://doi.org/10.1007/s10021-006-9013-8

Collister, J. W., Rieley, G., Stern, B., Eglinton, G., & Fry, B. (1994). Compound-specific $\delta^{13}C$ analyses of leaf lipids from plants with differing carbon dioxide metabolisms. *Organic Geochemistry*, *21*(6–7), 619–627. https://doi.org/10.1016/0146-6380(94)90008-6

Dean, W. E., & Gorham, E. (1998). Magnitude and significance of carbon burial in lakes, reservoirs, and peatlands. *Geology*, *26*(6), 535–538. https://doi.org/10.1130/0091-7613(1998)026<0535:MASOCB>2.3.CO;2

Diefendorf, A. F., & Freimuth, E. J. (2017). Extracting the most from terrestrial plant-derived *n*-alkyl lipids and their carbon isotopes from the sedimentary record: A review. *Organic Geochemistry*, *103*, 1–21. https://doi.org/10.1016/j.orggeochem.2016.10.016

Downie, A., Munroe, P., & Crosky, A. (2009). Characteristic of biochar: physical and structural properties. In J. Lehmann, & S. Joseph (Eds.), *Biochar for environmental management: Science and technology* (pp. 13–29). Earthscan.

Downing, J. A., Cole, J. J., Middelburg, J. J., Striegl, R. G., Duarte, C. M., Kortelainen, P., et al. (2008). Sediment organic carbon burial in agriculturally eutrophic impoundments over the last century. *Global Biogeochemical Cycles*, *22*(1), 1–10. https://doi.org/10.1029/2006GB002854

Drenzek, N. J., Montluçon, D. B., Yunker, M. B., Macdonald, R. W., & Eglinton, T. I. (2007). Constraints on the origin of sedimentary organic carbon in the Beaufort Sea from coupled molecular ^{13}C and ^{14}C measurements. *Marine Chemistry*, *103*(1–2), 146–162. https://doi.org/10.1016/j.marchem.2006.06.017

Droppo, L. G., Jeffries, D., Jaskot, C., & Backus, S. (1998). The prevalence of freshwater flocculation in cold regions: A case study from the Mackenzie River Delta. *Arctic*, *51*(2), 155–164. https://doi.org/10.14430/arctic1056

Dyke, L. D., & Brooks, G. R. (2000). *The physical environment of the Mackenzie Valley, Northwest Territories: A base line for the assessment of environmental change* (Vol. 6956, p 547). Geological Survey of Canada. Open File.

Eglinton, G., & Hamilton, R. J. (1967). Leaf epicuticular waxes. *Science*, *156*(3780), 1322–1335. https://doi.org/10.1126/science.156.3780.1322

Emmerton, C. A., Lesack, L. F. W., & Marsh, P. (2007). Lake abundance, potential water storage, and habitat distribution in the Mackenzie River Delta, western Canadian Arctic. *Water Resources Research*, *43*(5), 1–14. https://doi.org/10.1029/2006WR005139

Ferguson, M. E. (1990). Sediment movement in lakes in the centre area of the Mackenzie delta, N.W.T (Master's Thesis). University of Saskatchewan.

Freymond, C. V., Kündig, N., Stark, C., Peterse, F., Buggle, B., Lupker, M., et al. (2018). Evolution of biomolecular loadings along a major river system. *Geochimica et Cosmochimica Acta*, *223*, 389–404. https://doi.org/10.1016/j.gca.2017.12.010

Galy, V., France-Lanord, C., & Lartiges, B. (2008). Loading and fate of particulate organic carbon from the Himalaya to the Ganga-Brahmaputra delta. *Geochimica et Cosmochimica Acta*, *72*(7), 1767–1787. https://doi.org/10.1016/j.gca.2008.01.027

Goñi, M. A., Yunker, M. B., MacDonald, R. W., & Eglinton, T. I. (2005). Distribution and sources of organic biomarkers in arctic sediments from the Mackenzie River and Beaufort Shelf. *Marine Chemistry*, *71*(1–2), 23–51. https://doi.org/10.1016/S0304-4203(00)00037-2

Graf Pannatier, E. G. (1997). *Sediment accumulation and historical deposition of trace metals and trace organic compounds in the Mackenzie Delta (Northwest Territories, Canada)*. Université de Genève. https://doi.org/10.13097/archive-ouverte/unige:97977.

Hemingway, J. D., Schefuß, E., Spencer, R. G. M., Dinga, B. J., Eglinton, T. I., McIntyre, C., & Galy, V. V. (2017). Hydrologic controls on seasonal and inter-annual variability of Congo River particulate organic matter source and reservoir age. *Chemical Geology*, *466*(June), 454–465. https://doi.org/10.1016/j.chemgeo.2017.06.034

Hilton, R. G., Galy, V., Gaillardet, J., Dellinger, M., Bryant, C., O'Regan, M., et al. (2015). Erosion of organic carbon in the Arctic as a geological carbon dioxide sink. *Nature*, *524*(7563), 84–87. https://doi.org/10.1038/nature14653

Hobbs, W. O., Engstrom, D. R., Scottler, S. P., Zimmer, K. D., & Cotner, J. B. (2013). Estimating modern carbon burial rates in lakes using a single sediment sample. *Limnology and Oceanography: Methods*, *11*, 316–326. https://doi.org/10.4319/lom.2013.11.316

Holmes, R. M., McClelland, J. W., Peterson, B. J., Tank, S. E., Bulygina, E., Eglinton, T. I., et al. (2012). Seasonal and annual fluxes of nutrients and organic matter from large rivers to the Arctic Ocean and surrounding seas. *Estuaries and Coasts*, *35*(2), 369–382. https://doi.org/10.1007/s12237-011-9386-6

Holmes, R. M., Mcclelland, J. W., Tank, S. E., Spencer, R. G. M., & Shiklomanov, A. I. (2020). *Water quality dataset, version 20200421*. Arctic Great Rivers Observatory.

Jacobsen, S. B., & Wasserburg, G. J. (1980). Sm-Nd isotopic evolution of chondrites. *Earth and Planetary Science Letters*, *50*, 139–155.

Keil, R. G., Mayer, L. M., Quay, P. D., Richey, J. E., & Hedges, J. I. (1997). Loss of organic matter from riverine particles in deltas. *Geochimica et Cosmochimica Acta*, *61*(7), 1507–1511. https://doi.org/10.1016/S0016-7037(97)00044-6

Kvenvolden, K. A. (1966). Molecular distributions of normal fatty acids and paraffins in some lower cretaceous sediments. *Nature*, *209*, 573–577.

Lalonde, K., Mucci, A., Ouellet, A., & Gélinas, Y. (2012). Preservation of organic matter in sediments promoted by iron. *Nature Letter*, *483*, 198–200. https://doi.org/10.1038/nature10855.

Lesack, L. F. W., & Marsh, P. (2007). Lengthening plus shortening of river-to-lake connection times in the Mackenzie River Delta respectively via two global change mechanisms along the Arctic coast. *Geophysical Research Letters*, *34*(23), 1–6. https://doi.org/10.1029/2007GL031656

Lesack, L. F. W., & Marsh, P. (2010). River-to-lake connectivities, water renewal, and aquatic habitat diversity in the Mackenzie River Delta. *Water Resources Research*, *46*(12), 1–16. https://doi.org/10.1029/2010WR009607

Lesack, L. F. W., Marsh, P., Hicks, F. E., & Forbes, D. L. (2014). Local spring warming drives earlier river-ice breakup in a large Arctic delta. *Geophysical Research Letters*, *41*, 1560–1566. https://doi.org/10.1002/2013GL058761

Macdonald, R. W., Solomon, S. M., Cranston, R. E., Welch, H. E., Yunker, M. B., & Gobeil, C. (1998). A sediment and organic carbon budget for the Canadian beaufort shelf. *Marine Geology*, *144*(4), 255–273. https://doi.org/10.1016/S0025-3227(97)00106-0

Marsh, P., & Hey, M. (1989). The flooding hydrology of Mackenzie Delta lakes near Inuvik, NWT, Canada (Vol. *42*). Arctic Institute of North America. Retrieved from https://www.jstor.org/stable/i40022309

Marsh, P., & Hey, M. (1994). Analysis of spring high water events in the Mackenzie Delta and implications for lake and terrestrial flooding. *Geografiska Annaler: Series A , Physical Geography*, *76*(4), 221–234. https://doi.org/10.1080/04353676.1994.11880420

Marsh, P., Lesack, L. F. W., & Roberts, A. (1999). Lake sedimentation in the Mackenzie Delta, NWT. *Hydrological Processes*, *13*(16 SPEC), 2519–2536. https://doi.org/10.1002/(SICI)1099-1085(199911)13:16<2519::AID-HYP935>3.0.CO;2-T

Mayer, L. M. (1994). Surface area control of organic carbon accumulation in continental shelf sediments. *Geochimica et Cosmochimica Acta*, *58*(4), 1271–1284.

Mcclelland, J. W., Townsend-Small, A., Holmes, R. M., Pan, F., Stieglitz, M., Kosh, M., & Peterson, B. J. (2014). River export of nutrients and organic matter from the North Slope of Alaska to the Beaufort Sea. *Water Resources Research*, *50*, 1823–1839. https://doi.org/10.1002/2013WR014979.Reply

McIntyre, C., Wacker, L., Haghipour, N., Blattmann, T. M., Fahrni, S., Usman, M. O., et al. (2016). Online ^{13}C and ^{14}C gas measurements by EA-IRMS–AMS at ETH Zürich. *Radiocarbon*, *59*(3), 893–903. https://doi.org/10.1017/RDC.2016.68

Mendonça, R., Müller, R. A., Clow, D., Verpoorter, C., Raymond, P., Tranvik, L. J., & Sobek, S. (2017). Organic carbon burial in global lakes and reservoirs. *Nature Communications*, *8*(1), 1–6. https://doi.org/10.1038/s41467-017-01789-6

Meyers, P. A. (1994). Preservation of elemental and isotopic source identification of sedimentary organic matter. *Chemical Geology*, *114*(3–4), 289–302. https://doi.org/10.1016/0009-2541(94)90059-0

Peterse, F., Vonk, J. E., Holmes, R. M., Giosan, L., Zimov, N., & Eglinton, T. I. (2014). Branched glycerol dialkyl glycerol tetraethers in Arctic lake sediments: Sources and implications for paleothermometry at high latitudes. *Journal of Geophysical Research: Biogeosciences*, *119*, 1738–1754. https://doi.org/10.1002/2014JG002804.Received

Peterson, B. J., Holmes, R. M., McClelland, J. W., Vörösmarty, C. J., Lammers, R. B., Shiklomanov, A. I., et al. (2002). Increasing river discharge to the Arctic Ocean. *Science*, *298*(5601), 2171–2173. https://doi.org/10.1126/science.1077445

Peterson, B. J., McClelland, J., Curry, R., Holmes, R. M., Walsh, J. E., & Aagaard, K. (2006). Trajectory shifts in the arctic and subarctic freshwater cycle. *Science*, *313*(5790), 1061–1066. https://doi.org/10.1126/science.1122593

Pin, C., & Zaldguegui, J. F. S. (1997). Sequential separation of light rare-earth elements, thorium and uranium by miniaturized extraction chromatography: Application to isotopic analyses of silicate rocks. *Analytica Chimica Acta*, *339*, 79–89.

Raymond, P. A., Hartmann, J., Lauerwald, R., Sobek, S., Mcdonald, C., & Hoover, M. (2013). Global carbon dioxide emissions from inland waters. *Nature*, *503*(7476), 355–359. https://doi.org/10.1038/nature12760

Reimer, P., Bard, E., Bayliss, A., & Beck, J. W. (2013). IntCal13 and Marine13 radiocarbon age calibration curves 0–50,000 years cal BP. *Radiocarbon*, *55*(4), 1869–1887. https://doi.org/10.2458/azu_js_rc.55.16947

Rember, W. C., Erdman, T. W., Hoffmann, M. L., Chamberlain, V. E., & Sprenke, K. F. (1993). Dating of mine waste in lacustrine sediments using cesium-137. *Environmental Geology*, *22*(3), 242–245. https://doi.org/10.1007/BF00767409

Richter-Menge, J., Druckenmiller, M. L., & Jeffries, M. (2019). *Arctic report card 2019*. NOAA. Retrieved from https://www.arctic.noaa.gov/Report-Card

Sobek, S., Durisch-Kaiser, E., Zurbrügg, R., Wongfun, N., Wessels, M., Pasche, N., & Wehrli, B. (2009). Organic carbon burial efficiency in lake sediments controlled by oxygen exposure time and sediment source. *Limnology and Oceanography*, *54*(6), 2243–2254. https://doi.org/10.4319/lo.2009.54.6.2243

Sobek, S., Tranvik, L. J., & Cole, J. J. (2005). Temperature independence of carbon dioxide supersaturation in global lakes. *Global Biogeochemical Cycles*, *19*(2), 1–10. https://doi.org/10.1029/2004GB002264

Squires, M. M., & Lesack, L. F. W. (2002). Water transparency and nutrients as controls on phytoplankton along a flood-frequency gradient among lakes of the Mackenzie Delta, western Canadian Arctic. *Canadian Journal of Fisheries and Aquatic Sciences*, *59*(8), 1339–1349. https://doi.org/10.1139/f02-085

Squires, M. M., Lesack, L. F. W., Hecky, R. E., Guildford, S. J., Ramlal, P., & Higgins, S. N. (2009). Primary production and carbon dioxide metabolic balance of a lake-rich arctic river floodplain: Partitioning of phytoplankton, epipelon, macrophyte, and epiphyton production among lakes on the Mackenzie Delta. *Ecosystems*, *12*(5), 853–872. https://doi.org/10.1007/s10021-009-9263-3

Tank, S. (2009). Sources and cycling of Dissolved organic carbon across a landscape of Arctic delta lakes (PhD thesis). Simon Fraser University.

Tank, S. E., Lesack, L. F. W., & Hesslein, R. H. (2008). Northern Delta lakes as summertime CO_2 absorbers within the Arctic landscape. *Ecosystems*, *12*(1), 144–157. https://doi.org/10.1007/s10021-008-9213-5

Tank, S. E., Lesack, L. F. W., & Mcqueen, D. J. (2009). Elevated pH regulates bacterial carbon cycling in lakes with high photosynthetic activity. *Ecology*, *90*(7), 1910–1922. https://doi.org/10.1890/08-1010.1

Tao, S., Eglinton, T. I., Montluçon, D. B., McIntyre, C., & Zhao, M. (2015). Pre-aged soil organic carbon as a major component of the Yellow River suspended load: Regional significance and global relevance. *Earth and Planetary Science Letters*, *414*, 77–86. https://doi.org/10.1016/j.epsl.2015.01.004

Thirwall, M. F. (1991). Long-term reproducibility of multicollector Sr and Nd isotope ratio analysis. *Chemical Geology*, *94*, 85–104. https://doi.org/10.1016/0168-9622(91)90002-E

Tolosa, I., Fiorini, S., Gasser, B., Martín, J., & Miquel, J. C. (2013). Carbon sources in suspended particles and surface sediments from the Beaufort Sea revealed by molecular lipid biomarkers and compound-specific isotope analysis. *Biogeosciences*, *10*(3), 2061–2087. https://doi.org/10.5194/bg-10-2061-2013

Tranvik, L. J., Cole, J. J., & Prairie, Y. T. (2018). The study of carbon in inland waters-from isolated ecosystems to players in the global carbon cycle. *Limnology and Oceanography Letters*, *3*(3), 41–48. https://doi.org/10.1002/lol2.10068

Tranvik, L. J., Downing, J. A., Cotner, J. B., Loiselle, S. A., Striegl, R. G., Ballatore, T. J., et al. (2009). Lakes and reservoirs as regulators of carbon cycling and climate. *Limnology and Oceanography*, *54*(6 PART 2), 2298–2314. https://doi.org/10.4319/lo.2009.54.6_part_2.2298

Vance, D., & Thirwall, M. F. (2002). An assessment of mass discrimination in MC-ICPMS using Nd isotopes. *Chemical Geology*, *185*, 227–240. https://doi.org/10.1016/S0009-2541(01)00402-8

Vonk, J. E., Dickens, A. F., Giosan, L., Hussain, Z. A., Kim, B., Zipper, S. C., et al. (2016). Arctic deltaic lake sediments as recorders of fluvial organic matter deposition. *Frontiers in Earth Science*, *4*(August), 1–24. https://doi.org/10.3389/feart.2016.00077

Vonk, J. E., Drenzek, N. J., Hughen, K. A., Stanley, R. H. R., McIntyre, C., Montluçon, D. B., et al. (2019). Temporal deconvolution of vascular plant-derived fatty acids exported from terrestrial watersheds. *Geochimica et Cosmochimica Acta*, *244*, 502–521. https://doi.org/10.1016/j.gca.2018.09.034

Vonk, J. E., Giosan, L., Blusztajn, J., Montlucon, D., Graf Pannatier, E., McIntyre, C., et al. (2015). Spatial variations in geochemical characteristics of the modern Mackenzie Delta sedimentary system. *Geochimica et Cosmochimica Acta*, *171*, 100–120. https://doi.org/10.1016/j.gca.2015.08.005

Vonk, J. E., Tank, S. E., Bowden, W. B., Laurion, I., Vincent, W. F., Alekseychik, P., et al. (2015). Reviews and syntheses: Effects of permafrost thaw on Arctic aquatic ecosystems. *Biogeosciences*, *12*(23), 7129–7167. https://doi.org/10.5194/bg-12-7129-2015

Wakeham, S. T., Canuel, E. A., Lerberg, E. J., Mason, P., Sampere, T. P., & Bianchi, T. S. (2009). Partitioning of organic matter in continental margin sediments among density fractions. *Marine Chemistry*, *115*(3–4), 211–225. https://doi.org/10.1016/j.marchem.2009.08.005

Ward, N. D., Bianchi, T. S., Medeiros, P. M., Seidel, M., Richey, J. E., Keil, R. G., & Sawakuchi, H. O. (2017). Where carbon goes when water flows: Carbon cycling across the aquatic continuum. *Frontiers in Marine Science*, *4*, 1–27. https://doi.org/10.3389/fmars.2017.00007

Yunker, M. B., Backus, S. M., Graf Pannatier, E., Jeffries, D. S., & Macdonald, R. W. (2002). Sources and significance of alkane and PAH hydrocarbons in Canadian Arctic rivers.*Estuarine, Coastal and Shelf Science*, *55*(1), 1–31. https://doi.org/10.1006/ecss.2001.0880

Yunker, M. B., Macdonald, R. W., Cretney, W. J., Fowler, B. R., & McLaughlin, F. A. (1993). Alkane, terpene and polycyclic aromatic hydrocarbon geochemistry of the Mackenzie River and Mackenzie shelf: Riverine contributions to Beaufort Sea coastal sediment. *Geochimica et Cosmochimica Acta*, *57*(13), 3041–3061. https://doi.org/10.1016/0016-7037(93)90292-5